Available online at www.sciencedirect.com
ScienceDirect
Journal of Computational Physics 227 (2008) 3307–3321
JOURNAL OF COMPUTATIONAL PHYSICS
www.elsevier.com/locate/jcp

A numerical method for the study of nonlinear stability of axisymmetric flows based on the vector potential

J. Ortega-Casanova, R. Fernandez-Feria *

E.T.S. Ingenieros Industriales, Univ. Málaga, Pza. El Ejido s/n, 29013 Málaga, Spain

Received 9 October 2007; accepted 27 November 2007
Available online 8 December 2007

Abstract

We develop in this paper a numerical method to simulate three-dimensional incompressible flows based on a decomposition of the flow into an axisymmetric part, in terms of the stream function and the circulation, and a non-axisymmetric part in terms of a potential vector function. The method is specially suited for the study of nonlinear stability of axially symmetric flows because one may follow neatly the raising of the different non-axisymmetric modes, their nonlinear development, and their nonlinear interaction. The numerical technique combines finite differences on a non-uniform grid in the axial direction, a Chebyshev spectral collocation technique in the radial direction, and a Fourier spectral method in the azimuthal direction for the non-axisymmetric vector potential. As an example to check the efficiency and accuracy of the method we apply it to the flow inside a rotating circular pipe, and compare the resulting travelling waves with previous stability results for this problem, for different values of the Reynolds and the swirl numbers.

Keywords: Incompressible axisymmetric flow; Nonlinear stability; Vector potential

1. Introduction

Nonlinear stability analysis and the search for nonlinear wave solutions to the Navier–Stokes equations are fundamental tools for understanding the mechanisms underlying many flow transitions [1–3]. With the rapid advance in the speed and capacity of computers, and in the development of more efficient numerical techniques, these nonlinear analyses rely more and more in the direct numerical simulation of the three-dimensional (3D) Navier–Stokes equations (e.g. [4,5]).

We consider in this work the case of an incompressible flow which is axisymmetric in its basic state, and develop a numerical method that allows us to characterize the formation of instabilities, especially non-axisymmetric ones, their nonlinear development and their mutual interaction. As a matter of fact, any accurate numerical method able to solve the 3D Navier–Stokes equations written in cylindrical polar coordinates may perform this job. But if the variables and the numerical technique are not appropriate, the task of

* Corresponding author.
E-mail address: ramon.fernandez@uma.es (R. Fernandez-Feria).

0021-9991/$ - see front matter © 2007 Elsevier Inc. All rights reserved.
doi:10.1016/j.jcp.2007.11.041

isolating the raising of each individual nonlinear wave, and of tracking their interactions, may be quite difficult and time consuming, the more so the larger the number of unstable azimuthal modes involved.

One of the most efficient formulations to solve numerically the incompressible Navier–Stokes equations for axisymmetric (2D) flows is the so called stream function–circulation–vorticity (ψ–Γ–η) formulation (see e.g. [6,7]). In this formulation, the solenoidal constraint for the velocity field is automatically satisfied, the pressure is absent, and just two flow equations are needed, the azimuthal component of the vorticity equation for the stream function ψ, plus the azimuthal component of the momentum equation for the circulation Γ. However, to simplify the numerical integration, the first equation is decomposed into two equations, the azimuthal component of the vorticity equation in terms of the azimuthal vorticity component η itself, and a Poisson equation for ψ in terms of η [7]. A natural extension of this procedure to 3D flows is to add to the above axisymmetric description the non-axisymmetric part of the velocity field in terms of the vector potential $\mathbf{\Psi}$. Due to the definition of $\mathbf{\Psi}$, only two components of this functions are needed, which are governed by the remaining (radial and axial) components of the vorticity equation. However, as in the axisymmetric case, from a numerical point of view it is convenient to write these two equations in terms of the non-axisymmetric components of the vorticity vector, adding three new linear (Poisson) equations for them (see next section for the details).

Numerical methods for 3D viscous flows based in the vorticity-vector potential formulation have been widely used (e.g. [8–11]). Although the method has some drawbacks in relation to the primitive variables formulation, in particular, the increased number of equations to be handled and the complexity of the boundary conditions for the vorticity and the vector potential [9,12], it has some advantages for the porpoise of the present paper, where the objective is to separate neatly the non-axisymmetric components of the velocity and vorticity fields from their axisymmetric parts, because the axisymmetric part is much more easily computed from the ψ–Γ–η formulation. On the other hand, most of previous vector potential formulations use a solenoidal constraint for the vector potential and are discretized on staggered grids. But, again, for the porpoise of the present paper of separating the non-axisymmetric modes, it is more convenient to set to zero the azimuthal component of the vector potential, instead of the solenoidal constraint. This last technique has been successfully used in some linear stability analysis of axisymmetric flows [13,14]. In this paper, we extend this formulation to the whole nonlinear flow equations, and develop a numerical technique to solve them, discretizing the equations on a non-staggered, non-uniform grid in the radial and axial directions. This is combined with a Fourier series decomposition in the azimuthal direction, which permits the individual tracking of each azimuthal mode even in complicated non-axisymmetric flows.

To check the accuracy of the method we apply it to the flow in a rotating pipe, for which very abundant information is available in the literature on linear stability, nonlinear travelling waves, and numerical simulations [15–21]. In particular, Sanmiguel-Rojas and Fernandez-Feria [21] addresses the same problem but using a numerical technique based in primitive variables $(p, \mathbf{v})$ and Dirichlet boundary conditions for the pressure [22]. This technique is shown to be very efficient in detecting the raising and development of nonlinear instabilities from just numerical noise because only the two first azimuthal modes ($n = -1$ and $n = -2$) become unstable for the cases considered. However, for problems where many azimuthal modes are involved, the task of separating the contribution of each azimuthal mode and analyzing their mutual interaction may become cumbersome. On the other hand, from a physical point of view, the rotating pipe problem considered in this paper as a model problem is not exactly the same considered in Ref. [21], because in that reference the flow was driven by an axial pressure gradient, while in the present formulation the flow rate is kept constant and the pressure gradient is allow to vary. As noted previously by Toplosky and Akylas [18], these two formulations are not equivalent when finite-amplitude perturbations are involved.

2. Formulation

We use in this work non-dimensional variables in cylindrical polar coordinates (r, θ, z), where r and z are made dimensionless with a characteristic length scale L_c (a given radius of the problem, say). The velocity field in these coordinates, $\mathbf{v} = (u, v, w)$, which is made dimensionless with a characteristic velocity V_c, is split into two parts, an axisymmetric base flow, $\mathbf{V}(r, z, t)$, plus a perturbation field, $\mathbf{\Lambda}(r, \theta, z, t)$

$$\mathbf{v}(r, \theta, z, t) = \mathbf{V}(r, z, t) + \mathbf{\Lambda}(r, \theta, z, t). \tag{1}$$

Time t is made dimensionless with L_c/V_c. The base axisymmetric flow is solved through the stream function–circulation–vorticity formulation (see e.g. [7]):

$$\mathbf{V} \equiv (U, V, W)^{\mathrm{T}} = \nabla \wedge (\psi \mathbf{e}_\theta) + \frac{1}{r}\Gamma \mathbf{e}_\theta = \left(-\frac{1}{r}\frac{\partial \psi}{\partial z}, \frac{1}{r}\Gamma, \frac{1}{r}\frac{\partial \psi}{\partial r}\right)^{\mathrm{T}}, \tag{2}$$

where ψ is the stream function, Γ the circulation, and the superscript T means transposed. The deviation velocity $\mathbf{\Lambda}$ is written in terms of the potential vector $\mathbf{\Psi}(r, \theta, z, t)$

$$\mathbf{\Lambda} = \nabla \wedge \mathbf{\Psi}. \tag{3}$$

The fact that $\nabla \wedge \nabla \phi \equiv \mathbf{0}$ for any scalar function ϕ can be used to eliminate one of the components of $\mathbf{\Psi}$ (the θ-component, say), so that the potential vector can be written with just two components [13]

$$\mathbf{\Psi} = (\mathcal{G}, 0, \mathcal{F})^{\mathrm{T}}. \tag{4}$$

Therefore, the complete velocity field can be written as

$$\mathbf{v} = \begin{pmatrix} -\frac{1}{r}\partial_z \psi \\ \frac{1}{r}\Gamma \\ \frac{1}{r}\partial_r \psi \end{pmatrix} + \begin{pmatrix} \frac{1}{r}\partial_\theta \mathcal{F} \\ \partial_z \mathcal{G} - \partial_r \mathcal{F} \\ -\frac{1}{r}\partial_\theta \mathcal{G} \end{pmatrix}, \tag{5}$$

where ∂_i means partial derivative with respect to the variable i.

On the other hand, the vorticity vector is

$$\boldsymbol{\omega} \equiv (\omega_r, \omega_\theta, \omega_z)^{\mathrm{T}} = \nabla \wedge \mathbf{v} = \nabla \wedge \mathbf{V} + \nabla \wedge \mathbf{\Lambda} = \nabla \wedge \mathbf{V} + \nabla \wedge \nabla \wedge \mathbf{\Psi} = \nabla \wedge \mathbf{V} + \nabla \cdot (\nabla \mathbf{\Psi}^{\mathrm{T}} - \nabla \mathbf{\Psi}) \equiv \mathbf{\Omega} + \mathbf{\Theta}, \tag{6}$$

where $\mathbf{\Omega}$ is the axisymmetric part of the vorticity, given by

$$\mathbf{\Omega} \equiv \begin{pmatrix} \Omega_r \\ \Omega_\theta \\ \Omega_z \end{pmatrix} = \begin{pmatrix} -\partial_z V \\ \partial_z U - \partial_r W \\ \frac{1}{r}\partial_r (rV) \end{pmatrix} = \begin{pmatrix} -\frac{1}{r}\partial_z \Gamma \\ \eta \\ \frac{1}{r}\partial_r \Gamma \end{pmatrix} \tag{7}$$

and $\mathbf{\Theta}$ the non-axisymmetric part of the vorticity field, given by

$$\mathbf{\Theta} \equiv (\mathcal{X}, \mathcal{Y}, \mathcal{Z})^{\mathrm{T}} = \nabla \cdot (\nabla \mathbf{\Psi}^{\mathrm{T}} - \nabla \mathbf{\Psi}) = \begin{pmatrix} \partial_{rz}\mathcal{F} - \partial_{zz}\mathcal{G} - \frac{1}{r^2}\partial_{\theta\theta}\mathcal{G} \\ \frac{1}{r}\partial_{r\theta}\mathcal{G} - \frac{1}{r^2}\partial_\theta \mathcal{G} + \frac{1}{r}\partial_{\theta z}\mathcal{F} \\ \frac{1}{r}\partial_z \mathcal{G} + \partial_{rz}\mathcal{G} - \frac{1}{r}\partial_r \mathcal{F} - \partial_{rr}\mathcal{F} - \frac{1}{r^2}\partial_{\theta\theta}\mathcal{F} \end{pmatrix}. \tag{8}$$

In Eq. (7) we have defined $\eta \equiv \Omega_\theta$ as the azimuthal component of the axisymmetric part of the vorticity, which, together with ψ and Γ, completes the axisymmetric description of an incompressible flow in the stream function–circulation–vorticity formulation [7]. In terms of ψ, η is given by (from (2) and (7))

$$\eta = -\frac{1}{r}\nabla_*^2 \psi, \quad \nabla_*^2 \equiv \frac{\partial^2}{\partial z^2} + \frac{\partial^2}{\partial r^2} - \frac{1}{r}\frac{\partial}{\partial r}, \tag{9}$$

which constitutes a Poisson equation for ψ. The other two equations for the axisymmetric part of the velocity field $\mathbf{V}$ in this formulation are, respectively, the azimuthal component of the momentum equation for Γ, and the azimuthal component of the vorticity equation for η. These equations can be written, in non-dimensional form, as

$$\partial_t v = -u\partial_r v - \frac{v}{r}\partial_\theta v - w\partial_z v - \frac{uv}{r} + \frac{1}{Re}\left[\nabla^2 v + \frac{2}{r^2}\partial_\theta u - \frac{v}{r^2}\right], \tag{10}$$

$$\partial_t \omega_\theta = -u\partial_r \omega_\theta - \frac{v}{r}\partial_\theta \omega_\theta - w\partial_z \omega_\theta - \frac{v\omega_r}{r} + \omega_r \partial_r v + \frac{\omega_\theta}{r}\partial_\theta v + \omega_z \partial_z v + \frac{\omega_\theta u}{r} + \frac{1}{Re}\left[\nabla^2 \omega_\theta + \frac{2}{r^2}\partial_\theta \omega_r - \frac{\omega_\theta}{r^2}\right], \tag{11}$$

where

$$Re = \frac{V_c L_c}{\nu} \tag{12}$$

is the Reynolds number, with ν the kinematic viscosity of the fluid. Taking into account the following expressions for the velocity and vorticity components (from (5)–(8))

$$u = -\frac{1}{r}\partial_z\psi + \frac{1}{r}\partial_\theta\mathcal{F}, \quad v = \frac{\Gamma}{r} + \partial_z\mathcal{G} - \partial_r\mathcal{F}, \quad w = \frac{1}{r}\partial_r\psi + \frac{1}{r}\partial_\theta\mathcal{G}, \tag{13}$$

$$\omega_r = -\frac{1}{r}\partial_z\Gamma + \mathcal{X}, \quad \omega_\theta = \eta + \mathcal{Y}, \quad \omega_z = \frac{1}{r}\partial_z\Gamma + \mathcal{Z} \tag{14}$$

and substituting into (10) and (11), a set of two parabolic equations for the temporal evolution of Γ and η are obtained, which, in addition of ψ, Γ and η, also involve the *non-axisymmetric* variables $\mathcal{F}, \mathcal{G}, \mathcal{X}, \mathcal{Y}$ and $\mathcal{Z}$. Therefore, one needs five more equations for these unknowns, which are described next.

For $\mathcal{X}$ one uses the radial component of the vorticity equation, which can be written as

$$\partial_t\omega_r = -u\partial_r\omega_r - \frac{v}{r}\partial_\theta\omega_r - w\partial_z\omega_r - \frac{v\omega_\theta}{r} + \omega_r\partial_r u + \frac{\omega_\theta}{r}\partial_\theta u + \omega_z\partial_z u + \frac{\omega_\theta v}{r} + \frac{1}{Re}\left[\nabla^2\omega_r - \frac{2}{r^2}\partial_\theta\omega_\theta - \frac{\omega_r}{r^2}\right]. \tag{15}$$

Substituting (13) and (14), a parabolic equation for the temporal evolution of $\mathcal{X}$ is obtained. As for $\mathcal{Y}$, one uses the azimuthal component of (8), which can be written as

$$\mathcal{Y} \equiv \boldsymbol{\Theta}\cdot\mathbf{e}_\theta = \frac{1}{r}\partial_{r\theta}\mathcal{G} + \frac{1}{r}\partial_{\theta z}\mathcal{F} - \frac{1}{r^2}\partial_\theta\mathcal{G}. \tag{16}$$

This is an explicit equation for $\mathcal{Y}$, once $\mathcal{F}$ and $\mathcal{G}$ are known.

In the same way, the remaining axial component of the vorticity equation is used for $\mathcal{Z}$

$$\partial_t\omega_z = -u\partial_r\omega_z - \frac{v}{r}\partial_\theta\omega_z - w\partial_z\omega_z + \omega_r\partial_r w + \frac{\omega_\theta}{r}\partial_\theta w + \omega_z\partial_z w + \frac{1}{Re}[\nabla^2\omega_z], \tag{17}$$

which yields a parabolic equation for the temporal evolution of $\mathcal{Z}$ once (13) and (14) are substituted. Finally, for $\mathcal{F}$ and $\mathcal{G}$ one may use the radial and the axial components of (8), which can be written as

$$\mathcal{X} \equiv \boldsymbol{\Theta}\cdot\mathbf{e}_r = -\frac{1}{r^2}\partial_{\theta\theta}\mathcal{G} - \partial_{zz}\mathcal{G} + \partial_{rz}\mathcal{F}, \tag{18}$$

$$\mathcal{Z} \equiv \boldsymbol{\Theta}\cdot\mathbf{e}_z = -\partial_{rr}\mathcal{F} - \frac{1}{r^2}\partial_{\theta\theta}\mathcal{F} + \partial_{rz}\mathcal{G} + \frac{1}{r}\partial_z\mathcal{G} - \frac{1}{r}\partial_r\mathcal{F}. \tag{19}$$

One of the major difficulties in the vector potential formulation is the determination of the boundary conditions [9,23,24,12]. We discuss them in the context of the flow in a rotating pipe considered in Section 4.

3. Numerical method

3.1. Fourier decomposition

The non-axisymmetric variables (i.e., $\mathcal{X}, \mathcal{Y}, \mathcal{Z}, \mathcal{F}$, and $\mathcal{G}$), are *discretized* in the azimuthal direction θ by means of a complex Fourier decomposition as

$$\mathcal{F}(r,z,\theta,t) = \sum_{n=-\infty, n\neq 0}^{n=+\infty} \varphi_n(r,z,t)\mathrm{e}^{\mathrm{i}n\theta}, \tag{20}$$

$$\mathcal{G}(r,z,\theta,t) = \sum_{n=-\infty, n\neq 0}^{n=+\infty} \chi_n(r,z,t)\mathrm{e}^{\mathrm{i}n\theta}, \tag{21}$$

$$\mathcal{X}(r,z,\theta,t) = \sum_{n=-\infty, n\neq 0}^{n=+\infty} \alpha_n(r,z,t)\mathrm{e}^{\mathrm{i}n\theta}, \tag{22}$$

$$\mathcal{Y}(r,z,\theta,t) = \sum_{n=-\infty,n\neq 0}^{n=+\infty} \beta_n(r,z,t)\mathrm{e}^{\mathrm{i}n\theta}, \tag{23}$$

$$\mathcal{Z}(r,z,\theta,t) = \sum_{n=-\infty,n\neq 0}^{n=+\infty} \gamma_n(r,z,t)\mathrm{e}^{\mathrm{i}n\theta}, \tag{24}$$

where $\varphi_n, \chi_n, \alpha_n, \beta_n$, and γ_n are complex functions of (r,z,t). It must be noted that these variables are not defined for $n = 0$, since the axisymmetric mode is transferred into the axisymmetric variables ψ, Γ, and η.

From a numerical point of view, the infinite set of Fourier modes is truncated at some finite wavenumber N_θ. Thus, for instance, the two components of the potential vector are written as

$$\mathcal{F}(r,z,\theta,t) = \sum_{n=-N_\theta,n\neq 0}^{n=+N_\theta} \varphi_n(r,z,t)\mathrm{e}^{\mathrm{i}n\theta}, \quad \mathcal{G}(r,z,\theta,t) = \sum_{n=-N_\theta,n\neq 0}^{n=+N_\theta} \chi_n(r,z,t)\mathrm{e}^{\mathrm{i}n\theta}. \tag{25}$$

Therefore, for each one of these 3D variables there are $2N_\theta$ unknowns functions of (r,z,t), so that the same number of equations (i.e., $10 \times N_\theta$) must be provided. However, taking into account that the velocity and vorticity fields are obviously real fields, one has

$$f_{-n} = \hat{f}_n, \quad 1 \leqslant n \leqslant N_\theta, \tag{26}$$

where $f = \varphi, \chi, \alpha, \beta, \gamma$, and the hat denotes complex conjugate. This halves the number of unknown functions and equations associated to each non-axisymmetric variable.

To obtain these equations, we substitute the Fourier expansions into the equations described in the above section and equate terms multiplying $\mathrm{e}^{\mathrm{i}n\theta}$. For instance, substituting the Fourier expansions of $\mathcal{G}, \mathcal{F}$ and $\mathcal{Z}$ into (19), one obtains the following set of equations:

$$-\partial_{rr}\varphi_n + \frac{n^2}{r^2}\varphi_n + \partial_{rz}\chi_n + \frac{1}{r}\partial_z\chi_n - \frac{1}{r}\partial_r\varphi_n = \gamma_n, \quad 1 \leqslant n \leqslant N_\theta. \tag{27}$$

In the same way, from (18) and (16), one obtains

$$\frac{n^2}{r^2}\chi_n - \partial_{zz}\chi_n + \partial_{rz}\varphi_n = \alpha_n, \quad 1 \leqslant n \leqslant N_\theta, \tag{28}$$

$$\beta_n = \frac{\mathrm{i}n}{r}\partial_r\chi_n + \frac{\mathrm{i}n}{r}\partial_z\varphi_n - \frac{\mathrm{i}n}{r^2}\chi_n, \quad 1 \leqslant n \leqslant N_\theta. \tag{29}$$

The other linear equation is (9), which only involves axisymmetric variables, and which we rewrite here for completeness

$$\frac{1}{r}\partial_r\psi - \partial_{zz}\psi - \partial_{rr}\psi = r\eta. \tag{30}$$

The remaining equations are nonlinear evolution equations coming from (10), (11), (15) and (17). Using the orthogonality properties of $\mathrm{e}^{\mathrm{i}n\theta}$ together with (26), and truncating the Fourier expansions in N_θ, as stated above, one obtain the following equations:

$$\begin{aligned}\partial_t\Gamma = {} & \frac{1}{r}\partial_z\psi\partial_r\Gamma - \frac{1}{r}\partial_r\psi\partial_z\Gamma + \frac{1}{Re}\left(\partial_{rr}\Gamma - \frac{1}{r}\partial_r\Gamma + \partial_{zz}\Gamma\right) - \sum_{k+m=0}(\mathrm{i}k)\varphi_k\partial_{rz}\chi_m + \sum_{k+m=0}(\mathrm{i}k)\varphi_k\partial_{rr}\varphi_m \\ & - \sum_{k+m=0}\partial_z\chi_k(\mathrm{i}m)\partial_z\chi_m + \sum_{k+m=0}\partial_z\chi_k(\mathrm{i}m)\partial_r\varphi_m + \sum_{k+m=0}\partial_r\varphi_k(\mathrm{i}m)\partial_z\chi_m - \sum_{k+m=0}\partial_r\varphi_k(\mathrm{i}m)\partial_r\varphi_m \\ & + \sum_{k+m=0}(\mathrm{i}k)\chi_k\partial_{zz}\chi_m - \sum_{k+m=0}(\mathrm{i}k)\chi_k\partial_{rz}\varphi_m - \frac{1}{r}\sum_{k+m=0}(\mathrm{i}k)\varphi_k\partial_z\chi_m + \frac{1}{r}\sum_{k+m=0}(\mathrm{i}k)\varphi_k\partial_r\varphi_m,\end{aligned} \tag{31}$$

$$\begin{aligned}
\partial_t\eta = {} & \frac{1}{r}\partial_z\psi\partial_r\eta - \frac{1}{r}\partial_r\psi\partial_z\eta + \frac{2}{r^3}\Gamma\partial_z\Gamma - \frac{1}{r^2}\eta\partial_z\psi + \frac{1}{Re}\left(\partial_{rr}\eta + \frac{1}{r}\partial_r\eta + \partial_{zz}\eta - \frac{\eta}{r^2}\right) \\
& - \frac{1}{r}\sum_{k+m=0}(\mathrm{i}k)\varphi_k\partial_r\beta_m - \frac{1}{r}\sum_{k+m=0}\partial_z\chi_k(\mathrm{i}m)\beta_m + \frac{1}{r}\sum_{k+m=0}\partial_r\varphi_k(\mathrm{i}m)\beta_m + \frac{1}{r}\sum_{k+m=0}(\mathrm{i}k)\chi_k\partial_z\beta_m \\
& - \frac{1}{r}\sum_{k+m=0}\partial_z\chi_k\alpha_m + \frac{1}{r}\sum_{k+m=0}\partial_r\varphi_k\alpha_m + \sum_{k+m=0}\alpha_k\partial_{rz}\chi_m - \sum_{k+m=0}\alpha_k\partial_{rr}\varphi_m + \frac{1}{r}\sum_{k+m=0}\beta_k(\mathrm{i}m)\partial_z\chi_m \\
& - \frac{1}{r}\sum_{k+m=0}\beta_k(\mathrm{i}m)\partial_r\varphi_m + \sum_{k+m=0}\gamma_k\partial_{zz}\chi_m - \sum_{k+m=0}\gamma_k\partial_{rz}\varphi_m + \frac{1}{r^2}\sum_{k+m=0}\beta_k(\mathrm{i}m)\varphi_m, \qquad (32)
\end{aligned}$$

$$\begin{aligned}
\partial_t\alpha_n = {} & \frac{1}{r}\partial_z\psi\,\partial_r\alpha_n - \frac{\mathrm{i}n}{r}\left(\frac{1}{r^2}\partial_z\Gamma - \frac{1}{r}\partial_{rz}\Gamma\right)\varphi_n - \frac{\mathrm{i}n}{r^2}\Gamma\alpha_n - \frac{\mathrm{i}n}{r^2}\partial_{zz}\Gamma\chi_n - \frac{1}{r}\partial_r\psi\,\partial_z\alpha_n + \frac{\mathrm{i}n}{r^3}\partial_z\Gamma\varphi_n - \frac{\mathrm{i}n}{r^2}\partial_z\Gamma\,\partial_r\varphi_n \\
& + \alpha_n\left(\frac{1}{r^2}\partial_z\psi - \frac{1}{r}\partial_{rz}\psi\right) - \frac{n^2}{r^2}\eta\varphi_n + \frac{\mathrm{i}n}{r^2}\partial_r\Gamma\,\partial_z\varphi_n - \frac{1}{r}\partial_{zz}\psi\gamma_n \\
& + \frac{1}{Re}\left[\frac{1}{r}\partial_r\alpha_n + \partial_{rr}\alpha_n - \frac{n^2}{r^2}\alpha_n + \partial_{zz}\alpha_n - \frac{2\mathrm{i}n}{r^2}\beta_n - \frac{1}{r^2}\alpha_n\right] \\
& - \frac{1}{r}\sum_{k+m=n}(\mathrm{i}k)\varphi_k\,\partial_r\alpha_m - \frac{1}{r}\sum_{k+m=n}\partial_z\chi_k(\mathrm{i}m)\alpha_m \\
& + \frac{1}{r}\sum_{k+m=n}\partial_r\varphi_k(\mathrm{i}m)\alpha_m + \frac{1}{r}\sum_{k+m=n}(\mathrm{i}k)\chi_k\,\partial_z\alpha_m - \frac{1}{r^2}\sum_{k+m=n}\alpha_k(\mathrm{i}m)\varphi_m + \frac{1}{r}\sum_{k+m=n}\alpha_k(\mathrm{i}m)\partial_r\varphi_m \\
& - \frac{1}{r^2}\sum_{k+m=n}\beta_k m^2\varphi_m + \frac{1}{r}\sum_{k+m=n}\gamma_k(\mathrm{i}m)\partial_z\varphi_m, \quad 1 \leqslant n \leqslant N_\theta, \qquad (33)
\end{aligned}$$

$$\begin{aligned}
\partial_t\gamma_n = {} & \frac{1}{r}\partial_z\psi\,\partial_r\gamma_n - \frac{\mathrm{i}n}{r}\left(-\frac{1}{r^2}\partial_r\Gamma + \frac{1}{r}\partial_{rr}\Gamma\right)\varphi_n - \frac{\mathrm{i}n}{r^2}\Gamma\gamma_n + \frac{\mathrm{i}n}{r^2}\partial_{rz}\Gamma\chi_n - \frac{1}{r}\partial_r\psi\,\partial_z\gamma_n \\
& - \frac{\mathrm{i}n}{r^3}\partial_z\Gamma\chi_n + \frac{\mathrm{i}n}{r^2}\partial_z\Gamma\,\partial_r\chi_n + \alpha_n\left(-\frac{1}{r^2}\partial_r\psi + \frac{1}{r}\partial_{rr}\psi\right) + \frac{n^2}{r^2}\eta\chi_n - \frac{\mathrm{i}n}{r^2}\partial_r\Gamma\,\partial_z\chi_n + \frac{1}{r}\partial_{rz}\psi\gamma_n \\
& + \frac{1}{Re}\left[\frac{1}{r}\partial_r\gamma_n + \partial_{rr}\gamma_n - \frac{n^2}{r^2}\gamma_n + \partial_{zz}\gamma_n\right] - \frac{1}{r}\sum_{k+m=n}(\mathrm{i}k)\varphi_k\,\partial_r\gamma_m - \frac{1}{r}\sum_{k+m=n}\partial_z\chi_k(\mathrm{i}m)\gamma_m \\
& + \frac{1}{r}\sum_{k+m=n}\partial_r\varphi_k(\mathrm{i}m)\gamma_m + \frac{1}{r}\sum_{k+m=n}(\mathrm{i}k)\chi_k\,\partial_z\gamma_m + \frac{1}{r^2}\sum_{k+m=n}\alpha_k(\mathrm{i}m)\chi_m \\
& - \frac{1}{r}\sum_{k+m=n}\alpha_k(\mathrm{i}m)\partial_r\chi_m + \frac{1}{r^2}\sum_{k+m=n}\beta_k m^2\chi_m - \frac{1}{r}\sum_{k+m=n}\gamma_k(\mathrm{i}m)\partial_z\chi_m, \quad 1 \leqslant n \leqslant N_\theta. \qquad (34)
\end{aligned}$$

In these equations k and m vary in the interval $-N_\theta \leqslant k, m \leqslant +N_\theta$, with $k, m \neq 0$.

3.2. Discretization and numerical scheme

The set of $5N_\theta + 3$ scalar equations (27)–(34) given above, together with the corresponding boundary conditions to be discussed in the next section, are discretized in $N_r + 1$ nodes in the radial direction and $N_z + 1$ nodes in the axial direction. In particular, in the radial direction we use a Chebyshev pseudo-spectral collocation method [25], while in the axial direction a second-order finite-differences scheme on a non-uniform grid [26] is used, each one of them concentrating the nodes in the regions where the radial and axial gradients of the variables are the greatest.

The numerical scheme for solving the temporal evolution of the flow variables governed by the above set of coupled equations is the following. We first obtain the *axisymmetric* flow by solving (30)–(32) with appropriate boundary and initial conditions and setting all the non-axisymmetric variables to zero (i.e., using only the first lines in Eqs. (31) and (32)). The numerical procedure is very similar to that described in Ref. [7]. Given the

solution at a given instant $t = \tau\Delta t$, the temporal derivatives in (31) and (32) are approximated with a semi-implicit, two step predictor–corrector scheme with second order error in time. Viscous terms in these equations are discretized implicitly, while the convective terms explicitly. Once $\eta^{\tau+1}$ and $\Gamma^{\tau+1}$ are known, $\psi^{\tau+1}$ is obtained from the Poisson equation (30), which is solved with an ADI based technique, where the radial derivatives are discretized implicitly and the axial derivatives explicitly, and using standard solvers for band matrices with LU factorization from Blas and Lapack packages. The numerical procedure is started at $t = 0$ from some initial condition (e.g. the flow at rest) until an *axisymmetric* steady state is reached.

Once this axisymmetric steady state is obtained, we solve the whole set of non-axisymmetric equations with appropriate boundary conditions (see next section), and initial conditions given by the steady axisymmetric flow for ψ, Γ and η, together with random noise with a given intensity level for all the non-axisymmetric variables. Known the solution at a given instant τ, the parabolic equations (31) and (32) for Γ and η are solved as described above, but now including the non-axisymmetric terms in the right-hand side, together with the parabolic equations (33) and (34) for α_n and γ_n, which are solved with the same semi-implicit, two step predictor–corrector scheme used for Γ and η. With $\eta^{\tau+1}, \Gamma^{\tau+1}, \alpha_n^{\tau+1}$ and $\gamma_n^{\tau+1}$ known, $\psi^{\tau+1}$ is obtained from (30) as described above, while $\varphi_n^{\tau+1}$ and $\chi_n^{\tau+1}$ are solved from the similar Poisson-like equations (27), (28). These two sets of coupled equations are solved by means of an iterative SOR scheme (e.g. [12]), for which the optimum value of the under-relaxation factor is obtained with some preliminary tests. Finally, $\beta_n^{\tau+1}$ is obtained from (29), which is an explicit equation for β_n once φ_n and χ_n are known at the instant $\tau + 1$.

4. Flow in a rotating pipe. Boundary conditions

As a model problem to check the numerical technique described above we consider the rotating Hagen–Poiseuille flow (RHPF). Basically, a flow rate Q enters a pipe of unit radius (the characteristic length is then $L_c = R$, where R is the dimensional radius of the pipe) which rotates with angular velocity Ω. As the characteristic velocity we use $V_c = 2Q/(\pi R^2)$, fixed at the inlet section of the pipe $z = 0$; i.e., V_c is the maximum axial velocity at the axis in a Hagen–Poiseuille flow with flow rate Q, which is twice the mean velocity at the inlet section. Thus, the Reynolds number is the usual one in pipe flows, based on the mean velocity $(V_c/2)$ and the pipe diameter $(2R)$

$$Re \equiv \frac{V_c L_c}{\nu} = \frac{2Q}{\pi R \nu}. \tag{35}$$

The other physical parameter of the problem is the swirl number

$$S \equiv \frac{\Omega L_c}{V_c} = \frac{\pi \Omega R^3}{2Q}. \tag{36}$$

Alternatively, we use a rotation based Reynolds number Re_θ, instead of S, defined as

$$Re_\theta \equiv \frac{\Omega L_c^2}{\nu} = \frac{\Omega R^2}{\nu} = ReS. \tag{37}$$

There exists only one additional (geometrical) non-dimensional parameter associated to the pipe length, $L \equiv L_z/R$, where L_z is the dimensional length of the pipe. However, this parameter is irrelevant because we shall choose L large enough for the results to be independent of it (we shall use $L = 200$ in all the results reported in the next section).

We describe next the boundary conditions needed to solve the equations in the domain $0 \leqslant r \leqslant 1, 0 \leqslant \theta \leqslant 2\pi$, and $0 \leqslant z \leqslant L$, paying special attention to the boundary conditions for the components of the vorticity and the vector potential, which are not so intuitive as those for the velocity components or the stream function.

4.1. Inlet $(z = 0)$

In the inlet section of the pipe the velocity profile is given, and it is supposed to be axisymmetric, $\mathbf{v} = \mathbf{V}_{\text{in}} \equiv [U_{\text{in}}(r), V_{\text{in}}(r), W_{\text{in}}(r)]^{\text{T}}$. In particular, we shall assume that the flow enters the pipe with an unperturbed RHPF, i.e., $U_{\text{in}} = 0, V_{\text{in}} = Sr$, and $W_{\text{in}} = 1 - r^2$. Though we are going to use this inlet flow in

the computations reported in the next section, the formulation given below is also valid for a general axisymmetric velocity profile at the inlet, so that a different inlet velocity field $\mathbf{V}_{\rm in}$ may be used.

With this velocity profile, the axisymmetric variables ψ, Γ and η at the inlet are given by (see (2) and (9))

$$\psi_{\rm in}(r) = \int_0^r \varrho W_{\rm in}(\varrho)\mathrm{d}\varrho = \frac{r^2}{2}\left(1-\frac{r^2}{2}\right), \tag{38}$$

$$\Gamma_{\rm in}(r) = rV_{\rm in}(r) = Sr^2, \quad \eta_{\rm in}(r) = \partial_r W_{\rm in}(r) = -2r, \tag{39}$$

where it has been assumed that $\psi = 0$ at the axis.

On the other hand, since we assume that the perturbations vanish at the inlet

$$\mathbf{\Lambda}_{\rm in} = \nabla \wedge (\mathcal{F}_{\rm in}, 0, \mathcal{G}_{\rm in}) = \mathbf{0}, \tag{40}$$

using the definitions of their components through the Fourier expansions and Eq. (8), these conditions yield

$$\varphi_n = 0, \quad \chi_n = 0, \quad \partial_z\chi_n = 0, \quad \alpha_n = -\partial_{zz}\chi_n + \partial_{rz}\varphi_n, \quad \beta_n = \frac{\mathrm{i}n}{r}\partial_z\varphi_n, \quad \gamma_n = 0, \quad 1 \leqslant n \leqslant N_\theta. \tag{41}$$

4.2. Pipe wall ($r = 1$)

At the pipe wall both the axial and the radial velocity components vanish, and the azimuthal component is given by the rotation rate of the pipe, $V_R = V_{\rm in}\ (r = 1) = S$; i.e.,

$$\mathbf{v}_R = (0, V_R, 0)^{\rm T} = (-\partial_z\psi, \Gamma, \partial_r\psi)^{\rm T} + (\partial_\theta\mathcal{F}, \partial_z\mathcal{G} - \partial_r\mathcal{F}, -\partial_\theta\mathcal{G})^{\rm T}. \tag{42}$$

For the axisymmetric variables, taking into account the inlet conditions, one has

$$\psi = \psi_{\rm in}(r=1) = \frac{1}{4}, \quad \Gamma = V_R = S, \tag{43}$$

$$\eta = -\partial_{rr}\psi \quad \text{with } \partial_r\psi = 0. \tag{44}$$

For the non-axisymmetric part, making use of the Fourier expansions and integrating through the azimuthal direction taking into account the orthogonality properties of the Fourier modes, Eq. (42) together with Eq. (8) yield

$$\varphi_n = 0, \quad \chi_n = 0, \quad \partial_r\varphi_n = 0, \quad \alpha_n = 0, \quad \beta_n = \frac{\mathrm{i}n}{r}\partial_r\chi_n, \quad \gamma_n = \partial_{rz}\chi_n - \partial_{rr}\varphi_n, \qquad 1 \leqslant n \leqslant N_\theta. \tag{45}$$

4.3. Outflow ($z = L$)

For the axisymmetric variables ($n = 0$) the usual condition of quasi-cylindrical flow (see e.g. [27,28]) is used:

$$\partial_{zz}\psi = 0, \quad \partial_{zz}\Gamma = 0, \quad \partial_{zz}\eta = 0. \tag{46}$$

L should be large enough for the computed flow be independent of this boundary condition. For the remaining 3D variables we use a nonreflecting (radiation) boundary condition [29,30]

$$\partial_\theta f + C\partial_z f = 0, \quad f = \varphi_n, \chi_n, \alpha_n, \beta_n\gamma_n, \qquad 1 \leqslant n \leqslant N_\theta, \tag{47}$$

where the velocity C is set as the axial velocity at the axis ($r = 0$) of the base (axisymmetric) flow at the outlet section. Slight different values of C were checked without affecting appreciably to the results. As we shall see, this condition allows for the unconstraint exit of non-axisymmetric perturbations through the outlet section, avoiding numerical instabilities or spurious wave reflections [30].

4.4. Axis ($r = 0$)

Regularity at the axis yields the following boundary conditions:

$$\psi = 0, \quad \eta = 0, \quad \Gamma = 0,$$

$$\varphi_n = 0, \quad |n| = 1,$$
$$\varphi_n = \partial_r \varphi_n = 0, \quad |n| \neq 1,$$
$$\chi_n = \partial_r \chi_n = 0, \quad 1 \leqslant n \leqslant N_\theta,$$
$$\alpha_n = \begin{cases} \frac{1}{2}\partial_{rr}\chi_n + \partial_{rz}\varphi_n & \text{for } |n| = 1, \\ \frac{1}{2}\partial_{rr}\chi_n & \text{for } |n| \neq 1, \end{cases}$$
$$\beta_n = \begin{cases} (in)\left(\frac{1}{2}\partial_{rr}\chi_n + \partial_{rz}\varphi_n\right) & \text{for } |n| = 1, \\ (in)\left(\frac{1}{2}\partial_{rr}\chi_n\right) & \text{for } |n| \neq 1, \end{cases}$$
$$\gamma_n = \begin{cases} -\frac{3}{2}\partial_{rr}\varphi_n & \text{for } |n| = 1, \\ \partial_{rr}\varphi_n\left(\frac{n^2}{2} - 2\right) & \text{for } |n| \neq 1. \end{cases}$$

4.5. Initial conditions

As commented on above, we first obtain an axisymmetric steady state solution by integrating the axisymmetric equations (i.e., with the perturbations $\varphi_n, \chi_n, \alpha_n, \beta_n, \gamma_n$ set equal to zero in (30)–(32)). In the present example, this axisymmetric flow consists on a Hagen–Poiseuille flow superimposed to a rigid-body rotation, given by the inlet flow (38) and (39), which also coincides with the initial condition. Then we integrate the full non-axisymmetric equations (27)–(34) using this axisymmetric steady state solution as the initial conditions for the axisymmetric variables ψ, Γ, η, and a constant, very small, initial value ε for all the non-axisymmetric variables $\varphi_n, \chi_n, \alpha_n, \beta_n, \gamma_n$. In the results reported below we have used $\varepsilon = 10^{-10}$. As we shall see, this initial noise in the non-axisymmetric variables either goes to zero everywhere (within numerical round-off errors) if the axisymmetric flow is stable, or evolves to coherent travelling wave form if the flow is unstable.

5. Results

To check the accuracy of the numerical method and the numerical code we have selected $Re_\theta = 100$ and three values of the Reynolds numbers, $Re = 75$, 100, and 125 (they correspond to $S = 1.33$, 1, and 0.8, respectively). According to the linear stability theory for this problem, the first case ($Re = 75$ with $Re_\theta = 100$) is stable (see Fig. 1), the second one ($Re = 100$) is unstable, but just above the neutral curve, so that only the first non-axisymmetric mode $n = -1$ is unstable, while the third case ($Re = 125$) is well above the neutral curve, with two unstable modes, $n = -1$ and $n = -2$ (see Fig. 1).

In all the computations reported below we use $L = 200$ and five azimuthal modes ($N_\theta = 5$), which are shown to be enough to capture the evolution of all the raising non-axisymmetric perturbations (see below). In the radial and axial directions we use $N_r = 9$ and N_z between 200 and 1500, depending on the Reynolds number. We have checked the numerical results by using larger values of N_r and N_z in some computations. Finally, the Δt used lie in the interval 2.5×10^{-3}–5.0×10^{-3}, also depending on the Reynolds number.

The results are given in terms of the perturbation velocity $\mathbf{\Lambda}$, whose components can be written, from (5) and (25), (26), as

$$\Lambda_r = \frac{1}{r}\partial_\theta \mathcal{F} \simeq \frac{1}{r}\Re\left[\sum_{n=-N_\theta, n\neq 0}^{N_\theta} n\varphi_n e^{in\theta}\right], \tag{48}$$

$$\Lambda_\theta = \partial_z \mathcal{G} - \partial_r \mathcal{F} \simeq \Re\left[\sum_{n=-N_\theta, n\neq 0}^{N_\theta} (\partial_z \chi_n - \partial_r \varphi_n) e^{in\theta}\right], \tag{49}$$

$$\Lambda_z = -\frac{1}{r}\partial_\theta \mathcal{G} \simeq -\frac{1}{r}\Re\left[\sum_{n=-N_\theta, n\neq 0}^{N_\theta} n\chi_n e^{in\theta}\right]. \tag{50}$$

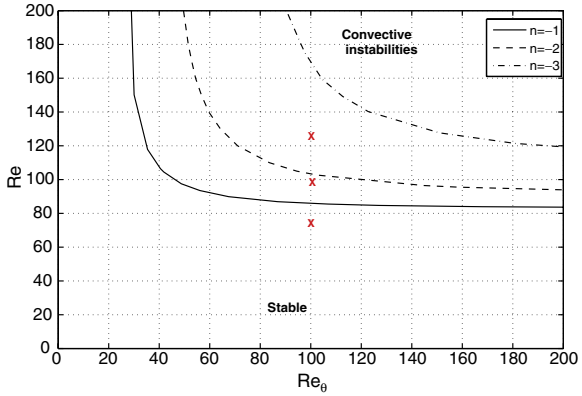

Fig. 1. Values of Re and Re_θ for the different numerical simulations considered (crosses) on a stability diagram. The lines represent the neutral curves for convective instabilities for different values of the azimuthal wavenumber n. The lower neutral curve for convective instability ($n = -1$) was first obtained by Mackrodt [16]; all the curves are taken from [17].

The results for $Re = 75$ are shown in Figs. 2 and 3. The initial non-axisymmetric perturbation, consisting on a constant noise of value $\varepsilon = 10^{-10}$, first decays and then develops into a coherent travelling wave that propagates downstream. As it is observed in Fig. 2, where Λ_r $(r = 0.75, \theta = [0, \pi], z, t)$ is plotted as a function of time t at four different axial locations z, the amplitude of this wave decays along the pipe, in accordance with the linear stability analysis (Fig. 1). In fact, the amplitude of the travelling wave decays more than four order of magnitude along the pipe (note the different scales in each part-figure of Fig. 2). This decay is better appreciated in Fig. 3, where we plot the maximum value throughout the pipe of each azimuthal component n of the different perturbation velocity components, $\Lambda_{r,n}$, $\Lambda_{\theta,n}$, and $\Lambda_{z,n}$. All the azimuthal components decay very fast, the faster the larger $|n|$. In fact, for this case we could have obtain practically the same results taking into account only the first two azimuthal modes ($N_\theta = 2$), because the remaining modes decay so fast to the round-off numerical error level that their contribution is completely negligible. As we shall see, the same can be said of all the remaining cases reported below. It is also worth mentioning that the outflow boundary condition used at $z = L = 200$ allows the free exit of the travelling waves formed inside the pipe (see Fig. 2(d)), without distorting or affecting them in any appreciable form.

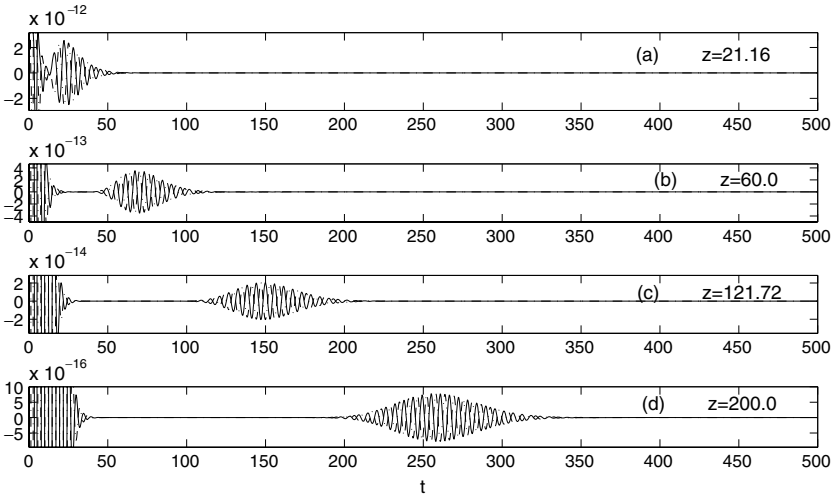

Fig. 2. Temporal evolution of the radial velocity perturbation Λ_r for $Re_\theta = 100$ and $Re = 75$ at $r = 0.75$, for $\theta = 0$ (continuous lines) and $\theta = \pi$ (dashed lines), and different axial locations z as indicated in each sub-figure.

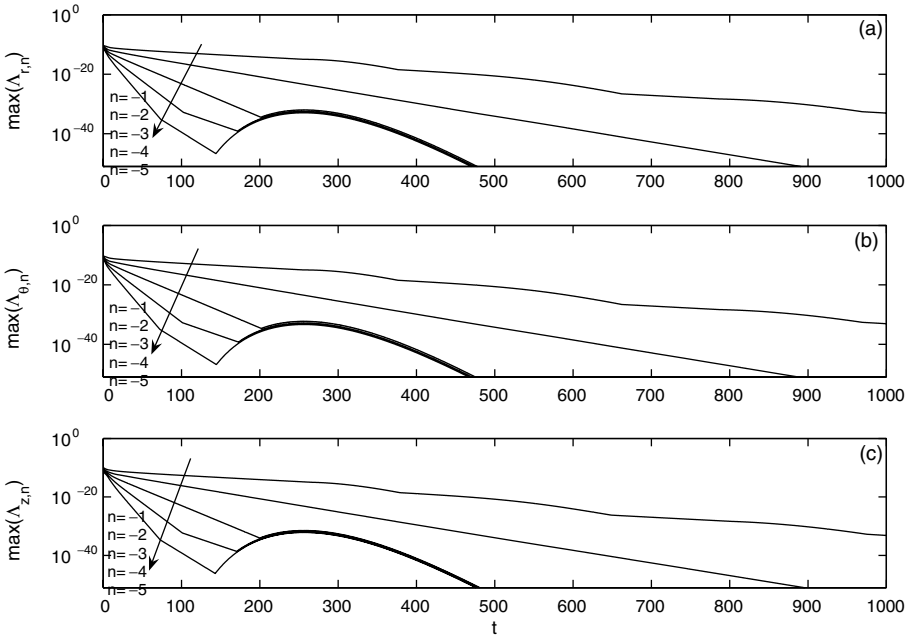

Fig. 3. Temporal evolution of the maximum values in the flow domain of the different azimuthal components (as indicated) of the radial velocity perturbation Λ_r (a), azimuthal velocity perturbation Λ_θ (b), and axial velocity perturbation Λ_z (c), for $Re_\theta = 100$ and $Re = 75$.

The following case $Re = 100$ is convectively unstable (see Fig. 1). The numerical results are shown in Figs. 4 and 5. The amplitude of the wave formed after the reorganization of the initial noise increases as it travels along the pipe (Fig. 4), but only slightly (just one order of magnitude) in agreement with the fact that this case is very close to the neutral curve (Fig. 1). Also in agreement with the linear stability analysis is the fact that only the azimuthal mode $n = -1$ is unstable: As shown in Fig. 5, the amplitude of the mode $n = -1$ increases until it saturates at $t \sim 275$ to $(\Lambda_{r,n})_{max} \simeq 3 \times 10^{-9}$, while all the remaining azimuthal modes decay in time.

To check the accuracy of the method we can compare quantitatively the numerical results for the frequency, the wavelength, and the group velocity of the perturbations with the predictions from the linear stability

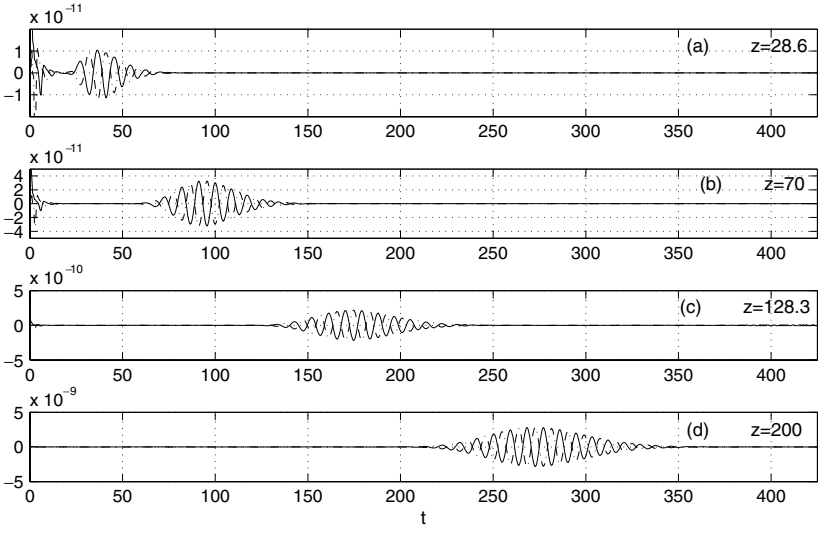

Fig. 4. As in Fig. 2, but for $Re = 100$.

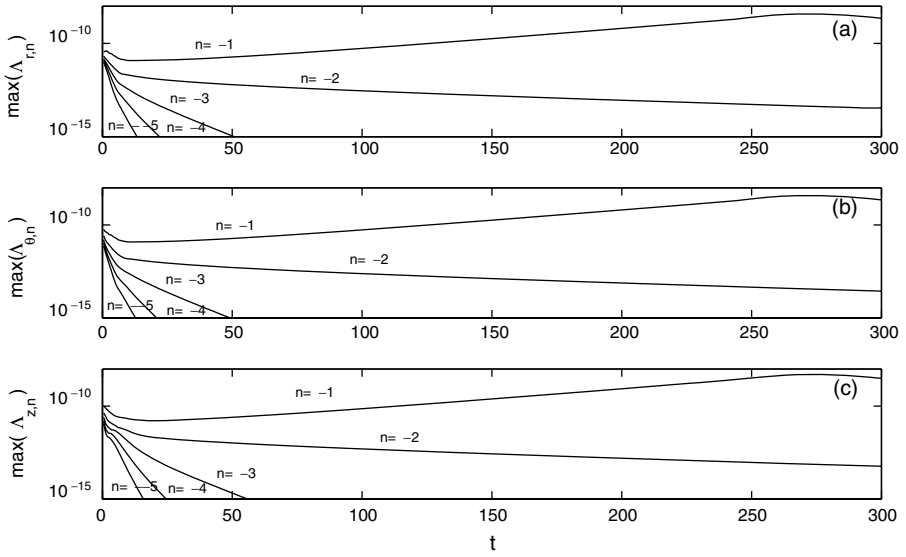

Fig. 5. As in Fig. 3, but for $Re = 100$.

theory. Thus, for instance, we can obtain the frequency of the amplifying travelling wave from Fig. 4(d), which is zoomed in Fig. 6. From it we obtain a non-dimensional period $T_N \simeq 8.894$, which yields a frequency $\omega_N = 2\pi/T_N \simeq 0.7065$. This value practically coincide with that corresponding to the most unstable frequency for the most unstable mode $n = -1$ obtained from the linear stability theory for this case $Re_\theta = 100$ and $Re = 100$ [17]: $\omega_S \simeq 0.7098$. The agreement is also very good for the wavenumber: From Fig. 7, which shows a picture of the travelling wave in the pipe at the instant $t = 130$, one may compute the non-dimensional wavelength of the travelling wave, $\lambda_N \simeq 13.72$, yielding a numerical wavenumber $\alpha_N = 2\pi/\lambda_N \simeq 0.4581$, very close to the linear stability value for the most unstable mode, $\alpha_S \simeq 0.432$. The agreement is better for the group velocity of the travelling waves, which from Fig. 4 can be computed to yield $c_N \simeq 0.734$, while the group velocity of the most unstable perturbation $n = -1$ from the linear stability theory is $c_S \simeq 0.730$ [17].

The results for the last case considered ($Re = 125$) are shown in Figs. 8 and 9. The axisymmetric flow is now more unstable than the former case and the amplitude of the travelling wave increases by five order of magnitude as it travels along the pipe (see Fig. 8). In addition, the mode $n = -2$ is also unstable in this case (see Fig. 9), in agreement with the linear stability analysis (Fig. 1). But the dominant unstable mode is still $n = -1$, which, according to Fig. 9, has an amplitude several order of magnitude larger than that of the mode $n = -2$

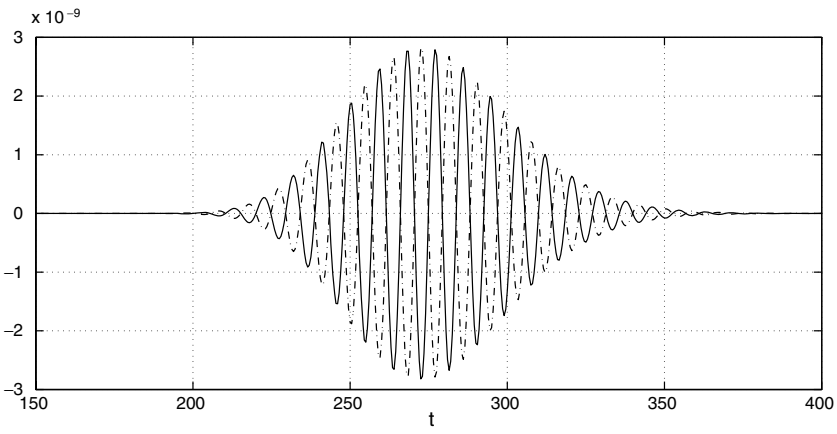

Fig. 6. Zoom of Fig. 4(d).

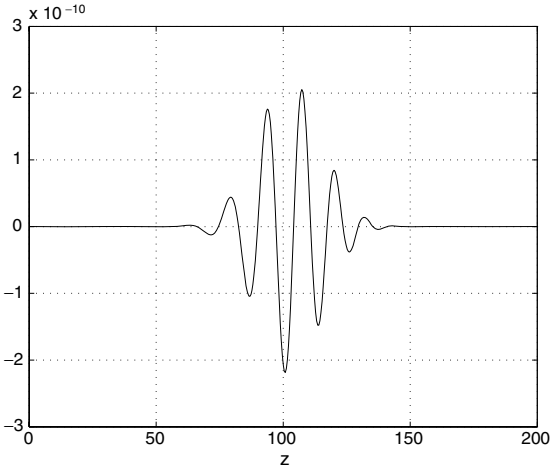

Fig. 7. Axial distribution along the axis $(r = 0, \theta = 0)$ of the radial velocity perturbation Λ_r at $t = 130$, for $Re_\theta = 100$ and $Re = 100$.

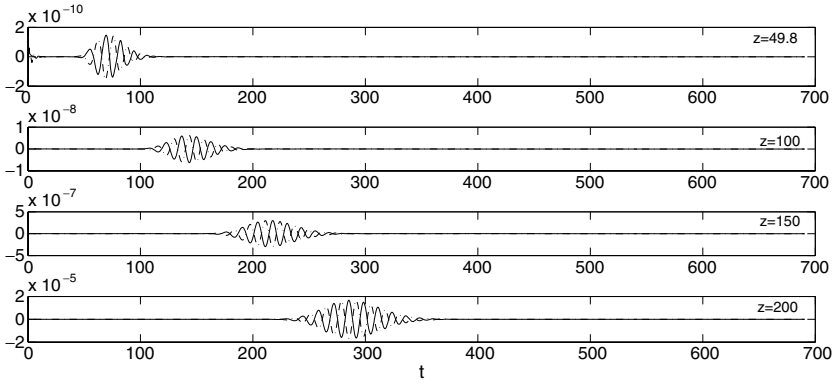

Fig. 8. As in Fig. 2, but for $Re = 125$.

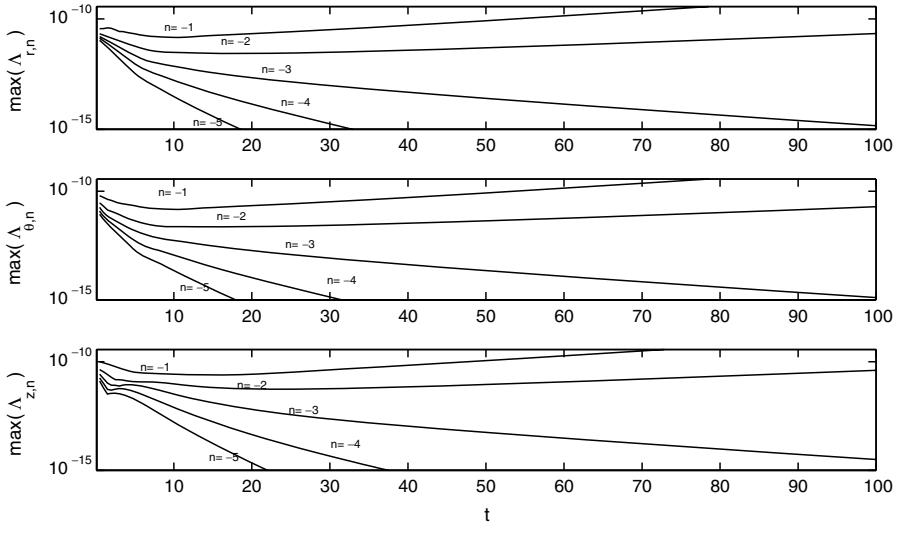

Fig. 9. As in Fig. 3, but for $Re = 125$.

for every time (the remaining modes $n = -3, -4, -5$ are stable and decay very fast in time). The frequency and group velocity of the travelling waves found numerically, $\omega_N \simeq 0.4822$ and $c_N \simeq 0.6745$, respectively, agree also very well with those obtained from the linear stability analysis for the most unstable mode with $n = -1$ [17]: $\omega_S \simeq 0.4811$ and $c_S \simeq 0.690$.

6. Conclusion

We have developed a numerical method for solving the incompressible Navier–Stokes equations in cylindrical polar coordinates based in the stream function–circulation–azimuthal vorticity formulation for the axisymmetric part, and on the vector potential–vorticity formulation for the non-axisymmetric part. The method is specially suited for the study of nonlinear stability of axisymmetric flows because the axisymmetric base flow is straightforwardly obtained at very low numerical cost, and because the evolution of each non-axisymmetric unstable mode can be easily followed separately. We have checked the accuracy and efficiency of the method by applying it to the flow in a rotating pipe, finding an excellent quantitative agreement between the non-axisymmetric travelling waves arising numerically for several Reynolds numbers with the predictions from stability theory. Although the formulation of the method is rather involved in comparison with, for instance, a method based in primitive variables, especially in relation to the boundary conditions, it has advantages for problems where many azimuthal modes become unstable, because their nonlinear development and mutual interactions can be followed as easily as in problems where just the few first azimuthal modes become unstable (such as the rotating pipe example considered here). Thus, we think that the method may have some advantages in relation to other available numerical methods for the study of nonlinear stability in complex swirling jets and wakes at moderately high Reynolds numbers.

Acknowledgments

This research has been supported by the Ministerio de Educación y Ciencia of Spain (grants FIS2004-00538, and FIS2007-60161) and by the European Commission (grant COOP-CT-2005-017725). The numerical computations were performed in the computer facility "Taylor" at the ETSII of the University of Málaga.

References

[1] P.J. Schmid, D.S. Henningson, Stability and Transition in Shear Flows, Springer, New York, 2001.
[2] W.S. Saric, H.L. Reed, E.B. White, Stability and transition of three-dimensional boundary layers, Annu. Rev. Fluid Dyn. 35 (2003) 413–440.
[3] R.R. Kerswell, Recent progress in understanding the transition to turbulence in a pipe, Nonlinearity 18 (2005) R17–R44.
[4] I. Dellbende, M. Rossi, Nonlinear evolution of a swirling jet instability, Phys. Fluids 17 (2005) 044103.
[5] E. Sanmiguel-Rojas, R. Fernandez-Feria, Nonlinear instabilities in a vertical pipe flow discharging from acylindrical container, Phys. Fluids 18 (2006) 024101.
[6] J.M. Lopez, Axisymmetric vortex breakdown. Part 1. Confined swirling flow, J. Fluid Mech. 221 (1990) 533–552.
[7] J.M. Lopez, P.D. Weidman, Stability of stationary end wall boundary layers during spin-down, J. Fluid Mech. 326 (1996) 373–398.
[8] K. Aziz, J.D. Hellums, Numerical solution of the three-dimensional equation of motion for laminar natural convection, Phys. Fluids 10 (1967) 314–324.
[9] A.K. Wong, J.A. Reizes, An effective vorticity–vector potential formulation for the numerical solution of three-dimensional duct flow problems, J. Comput. Phys. 55 (1984) 98–114.
[10] O.R. Tutty, On vector potential–vorticity methods for incompressible flow problems, J. Comput. Phys. 64 (1986) 368–379.
[11] W.E., J.-G. Liu, Finite difference methods for 3D viscous incompressible flows in the vorticity–vector potential formulation on nonstaggered grids, J. Comput. Phys. 138 (1997) 57–82.
[12] P.J. Roache, Fundamentals of Computational Fluid Dynamics, Hermosa, 1998.
[13] H.F. Goldstein, E. Knobloch, I. Mercader, M. Net, Convection in a rotating cylinder. Part I: Linear theory for moderate Prandtl numbers, J. Fluid Mech. 248 (1993) 583–604.
[14] Y. Spasov, J. Herrero, F.X. Grau, F. Giralt, Linear stability and numerical calculations of the lid-driven flow in a toroidal shaped cavity, Phys. Fluids 15 (2003) 134–146.
[15] T.J. Pedley, On the instability of viscous flow in a rapidly rotating pipe, J. Fluid Mech. 35 (1969) 97–115.
[16] P.A. Mackrodt, Stability of Hagen–Poiseuille flow with superimposed rigid rotation, J. Fluid Mech. 73 (1976) 153–164.
[17] R. Fernandez-Feria, C. del Pino, The onset of absolute instability of rotating Hagen–Poiseuille flow: a spatial stability analysis, Phys. Fluids 14 (2002) 3087–3097.

[18] N. Toplosky, T.R. Akylas, Nonlinear spiral waves in rotating pipe flow, J. Fluid Mech. 190 (1988) 39–54.
[19] D.R. Barnes, R.R. Kerswell, New results in rotating Hagen–Poiseuille flow, J. Fluid Mech. 417 (2000) 103–126.
[20] H. Wedin, R.R. Kerswell, Exact coherent structures in pipe flow: travelling wave solutions, J. Fluid Mech. 508 (2004) 333–371.
[21] E. Sanmiguel-Rojas, R. Fernandez-Feria, Nonlinear waves in the pressure driven flow in a finite rotating pipe, Phys. Fluids 17 (2005) 014104.
[22] R. Fernandez-Feria, E. Sanmiguel-Rojas, An explicit projection method for solving incompressible flows driven by a pressure difference, Comput. Fluids 33 (2004) 463–483.
[23] A.K. Wong, J.A. Reizes, The vector potential in the numerical solution of three-dimensional fluid dynamics problems in multiply connected regions, J. Comput. Phys. 62 (1986) 124–142.
[24] F. Marques, On boundary conditions for velocity potentials in confined flows: application to Couette flow, Phys. Fluids A 2 (1990) 729–737.
[25] C. Canuto, M.Y. Hussaini, A. Quarteroni, T.A. Zang, Spectral Methods in Fluid Dynamics, Springer-Verlag, New York, 1988.
[26] E. Sanmiguel-Rojas, J. Ortega-Casanova, C. del Pino, R. Fernandez-Feria, A cartesian grid finite-difference method for 2D incompressible viscous flows in irregular geometries, J. Comput. Phys 204 (2005) 302–318.
[27] P. Beran, F. Culik, The role of nonuniqueness in the development of vortex breakdown in tubes, J. Fluid Mech. 242 (1992) 491–597.
[28] J.M. Lopez, On the bifurcation structure of axisymmetric vortex breakdown in a constricted pipe, Phys. Fluids 6 (1994) 3683–3693.
[29] G. Jin, M. Braza, A nonreflecting outlet boundary condition for incompressible unsteady Navier–Stokes calculations, J. Comput. Phys. 107 (1993) 239–253.
[30] M.R. Ruith, P. Chen, E. Meiburg, Development of boundary conditions for direct numerical simulations of three-dimensional vortex breakdown in semi-infinite domains, Comput. Fluids 33 (2004) 1225–1250.